Research Article

Longshi Rao*, Qing Zhang, Mingfu Wen, Zhongfa Mao, Huaxian Wei, Han-Jui Chang, and Xiaodong Niu*

Solvent regulation synthesis of single-component white emission carbon quantum dots for white light-emitting diodes

https://doi.org/10.1515/ntrev-2021-0036
received May 8, 2021; accepted May 29, 2021

Abstract: White light-emitting diodes (WLEDs) hold great promise in lighting, display, and visible light communication devices, and single-component white emission carbon quantum dots (SCWE-CQDs) as the key component of WLEDs have many outstanding advantages. However, rapid and efficient synthesis of SCWE-CQDs with high photoluminescence quantum yield (PLQY) and stability remains challenging. Here, we report a novel solvent engineering strategy to obtain highly photoluminescent SCWE-CQDs by controlling the dilution ratios between *N*,*N*-dimethylformamide (DMF) and pristine red carbon quantum dots (RCQDs) solution. By optimizing synthesis conditions, the relative PLQY of the SCWE-CQDs solution reached 53%. Morphological, structural, and optical property characterizations indicate that the combined action of the hydrogen bond (HB) effect and the size effect leads to the blue shift of RCQDs, but the HB effect is more dominant than the particle size in causing large spectral shifts. In addition, the WLEDs with high color rendering index of 89 and remarkable reliability were obtained based on the highly photoluminescent SCWE-CQDs. This facile solvent engineering approach for synthesizing tunable emission CQDs will promote the progress of carbon-based luminescent materials for applications in optoelectronic devices.

Keywords: single-component white emission, carbon quantum dots, DMF regulation, white light-emitting diodes

1 Introduction

Phosphor-converted white light-emitting diodes (WLEDs) have emerged as an indispensable light source in the fields of illumination, display, and visible light communication because of their competitive advantages, including fast response speed, high energy efficiency, long lifetime, and low power consumption [1–3]. Currently, most available WLEDs are fabricated by combining blue emissive LED chips with green/yellow phosphors to generate white light [4–6]. Unfortunately, these WLEDs devices usually suffer from some unavoidable drawbacks, such as phase separation, self-absorption, fabrication complexity, and color fading over time [7]. In addition, due to the lack of red emission in the visible spectrum, the corresponding WLEDs devices exhibit a relatively low color rendering index (CRI), and the excess blue light originating from LED chips would evoke fatal retinal injury [8].

Recently, a promising strategy, adopted for overcoming the above issues and further achieving high color quality, is to develop ultraviolet (UV) pumped WLEDs with single-component white light emitters. Moreover, this strategy can not only reduce the blue light hazards of blue-chip WLEDs, but also filter out excess UV light without affecting the quality of the output white light. As a key component of WLEDs, single-component white materials mainly include rare-earth-based materials, organometallic complexes, and organic nonmetallic compounds [9–11]. However, these materials have usually encountered a series of issues, such as toxicity, low thermal/optical stability, high cost, environmental sensitivity, and complex fabrication procedures, which seriously

* **Corresponding author: Longshi Rao,** Department of Mechanical Engineering, College of Engineering, Shantou University, Shantou 515063, China; Intelligent Manufacturing Key Laboratory of Ministry of Education, Shantou University, Shantou 515063, China, e-mail: lsrao@stu.edu.cn
* **Corresponding author: Xiaodong Niu,** Department of Mechanical Engineering, College of Engineering, Shantou University, Shantou 515063, China; Intelligent Manufacturing Key Laboratory of Ministry of Education, Shantou University, Shantou 515063, China, e-mail: xdniu@stu.edu.cn
Qing Zhang, Mingfu Wen, Zhongfa Mao, Huaxian Wei, Han-Jui Chang: Department of Mechanical Engineering, College of Engineering, Shantou University, Shantou 515063, China; Intelligent Manufacturing Key Laboratory of Ministry of Education, Shantou University, Shantou 515063, China

block their practical applications in high-quality lighting and displays [12,13]. Therefore, it is of great significance to develop novel single-component white light emitters that overcome the above-mentioned shortcomings.

Nowadays, low-dimensional carbon nanomaterials mainly include zero-dimensional carbon quantum dots (CQDs), one-dimensional carbon nanotubes, and two-dimensional carbon nanoribbons, which have the characteristics of small size, large specific scale, and good mechanical performance [14–17]. Among these materials, luminescent CQDs have been taken delight in the photoelectric devices due to their unique and fascinating properties, including excellent stability, good biocompatibility, low production cost, and environmental friendliness [18–20]. In addition, compared with other single-component light emitters, single-component white emission CQDs (SCWE-CQDs) exhibit innate advantages in no phase separation, no color fading over time, and simple device fabrication process, which make them promising candidates for single-component WLEDs [21–23]. To date, heteroatom doping and surface modification have been the most commonly used methods to obtain SCWE-CQDs. Heteroatom doping (for example, S, N, or S, N-codoped) is an effective approach to modulate the surface states in CQDs to achieve single-component white emission, which is due to its special electronic structures and electronegativity [21]. However, the photoluminescence mechanism of CQDs is still unclear, which makes it difficult to regulate the properties of CQDs in control. Surface modification, mainly including chemical oxidation, amine group surface functionalization, surface treatment, and surface passivation of organic molecules, has attracted intensive attention for preparing SCWE-CQDs. For instance, Yuan *et al.* demonstrated the single-component white emission CQDs derived from blue-yellow fluorescence-phosphorescence dual emission with a photoluminescence quantum yield (PLQY) of 25% [22]. Dang *et al.* reported the fluorescent SCWE-CQDs that showed bright white fluorescence with a PLQY of 28.3% after ultrasonic treatment [24]. Moreover, Zhu *et al.* proposed an effective strategy for synthesizing SCWE-CQDs with a PLQY of 38.7% by modulating the emitting states of CQDs [25]. It is worth noting that the fluorescence quenching caused by CQDs aggregation in the solid state would still be considered a great breakthrough. Recent studies suggest that physical attachment, long-chain ligands grafting, and polymer coating can reduce the aggregation and improve the PLQY of CQDs. For example, Zhang *et al.* used *N*-(*b*-aminoethyl)-*g*-aminopropyl methldimethoxy silane (AEAPMS) as a passivator to avoid the SCWE-CQDs fluorescence quenching [26]. Despite many efforts to explore SCWE-CQDs, SCWE-CQDs still encounter many challenges, namely (i) quickly and easily synthesize SCWE-CQDs with high PLQY, and (ii) achieve high CRI (CRI >80) in WLEDs, especially for warm WLEDs, and (iii) avoid solid-state fluorescence quenching. Thus, a study for such material is highly desirable.

Motivated by the above-mentioned issues, in this work, we demonstrate a novel solvent engineering strategy to obtain highly photoluminescent and stable SCWE-CQDs *via* tuning red CQDs (RCQDs) properties with *N*,*N*-dimethylformamide (DMF). The characterization results prove that by controlling the dilution ratios between DMF and the original RCQDs solution, SCWE-CQDs can be obtained, with a PLQY as high as 53%. In order to understand the mechanism of DMF induction, we studied the relationship between spectrum shift and electron transmissions and found that the combined effect of the hydrogen bond (HB) effect and the size effect led to the blue shift of RCQDs, but the HB effect is dominant over particle size in causing the large spectral shift. Additionally, *N*-(*b*-aminoethyl)-*g*-aminopropyl methldimethoxy silane was chosen as the dispersing medium and protective material to avoid aggregation-induced fluorescence self-quenching of the SCWE-CQDs. Benefiting from these high-performance SCWE-CQDs, the WLEDs devices with a high CRI of 89 and remarkable reliability were obtained, demonstrating that the SCWE-CQDs are promising for applications in WLEDs of the ideal low-cost displays, illumination, and visible light communication devices.

2 Materials and methods

2.1 Chemicals and materials

Ammonium citrate (AC, A.R.), *N*,*N*-dimethylformamide (DMF, 99.8%), *N*-(*b*-aminoethyl)-*g*-aminopropyl methldimethoxy silane (AEAPMS, 96%), petroleum ether (PE, A.R.), and cellulose acetate (CA) were purchased from Aladdin Biochemical Technology Co., Ltd (Shanghai, China). All chemical reagents were used as received without further purification. Deionized water (18.2 MΩ) was used for all experiments.

2.2 Synthesis of RCQDs and SCWE-CQDs

In a typical process for the synthesis of RCQDs, 5.2 g AC was dissolved in 50 mL of DMF with vigorous stirring to achieve a homogeneous solution. After that, the solution was transferred to a 100 mL Teflon-lined stainless steel

autoclave and heated at 200°C for 6 h, resulting in a dark-red solution. Subsequently, the products were purified with PE three times to remove impurities and were dialyzed (1,000 Da of cut-off molecular weight) for 24 h to eliminate the unreacted precursor. Finally, a red small molecular sol was obtained. To prepare SCWE-CQDs, 1.0 mL RCQDs were added into 10 mL AEAPMS, followed by slight stirring at room temperature. Afterward, the mixture was diluted by DMF to produce the SCWE-CQDs. Before testing, the products were also purified with PE three times to remove impurities. The graphical abstract is shown in Figure 1.

2.3 Fabrication of SCWE-CQDs WLEDs devices

To evaluate the performance of SCWE-CQDs application in WLEDs, the CA with different contents was added into as-prepared SCWE-CQDs solution and then intensely stirred in a vacuum mixer for 6 minutes to degas bubbles. Afterward, the mixture was added dropwise to a 395 nm ultraviolet LED (UV-LED) chip and solidified at 130°C for 2 h under ambient conditions. The CCT, CRI, CIE color coordinates, and emission spectra of the WLEDs devices were characterized by using a high-accuracy integrating sphere system (Multi Spectrums T-950/930).

2.4 Characterization

TEM observation was performed on a transmission electron microscope (TEM, JEM-2100F, JEOL, Japan) with a 200 kV accelerating voltage. XRD patterns were recognized with an X-ray diffractometer (XRD, D8-Advance, Bruker, Germany) using a Cu-Kα radiation source. Absorption and fluorescence spectra were collected using an UV-visible spectrometer (Tu-1901, Purkinje, China) and a fluorescence spectrophotometer (RF-6000, Shimadzu, Japan) at room temperature, respectively. FTIR spectra were recorded from 4,000 to 400 cm^{-1} on a Fourier Transform Infrared Spectrometer (Vertex 33, Bruker, Germany). XPS data were obtained with an X-ray photoelectron spectrometer (XPS, Kratos Axis Ultra DLD, Kratos, UK) under a mono Al-Kα excitation source. The PLQY of CQDs solutions were determined by utilizing the following equation [19].

$$Q = Q_{st} \cdot \frac{I}{I_{st}} \cdot \frac{A}{A_{st}} \cdot \frac{n^2}{n_{st}^2} \quad (1)$$

where the Q is the PLQY, the subscript "st" denotes the reference quinine sulfate, "I" is the integrated fluorescence intensity, "A" is the UV-Vis absorbance at 365 nm, "n" is the different refractive index of the solvent, and the superscript "2" means the square of "n". Quinine sulfate dissolved in 0.1 M H_2SO_4 (PLQY: 55%) was used as the standard.

3 Results and discussion

3.1 Morphological and structural characterizations of RCQDs and SCWE-CQDs

The morphological and structural characterizations of as-prepared RCQDs and SCWE-CQDs were measured by

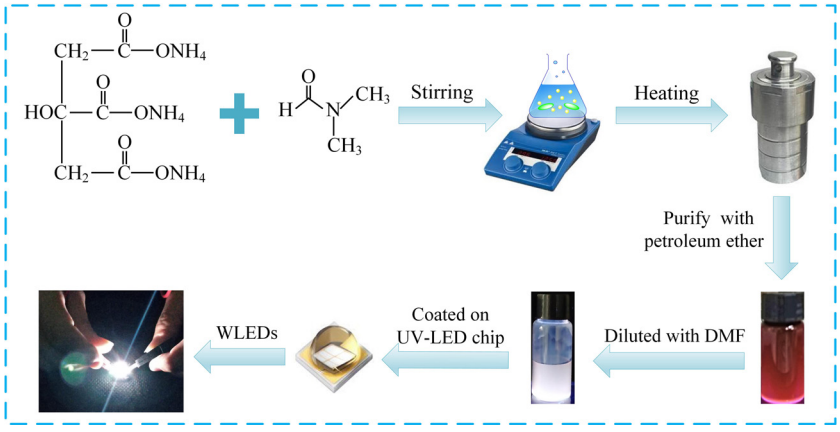

Figure 1: Schematic illustration of the preparation of RCQDs and SCWE-CQDs using a facile hydrothermal method with ammonium citrate (AC), *N*,*N*-dimethylformamide (DMF), and their application in WLEDs.

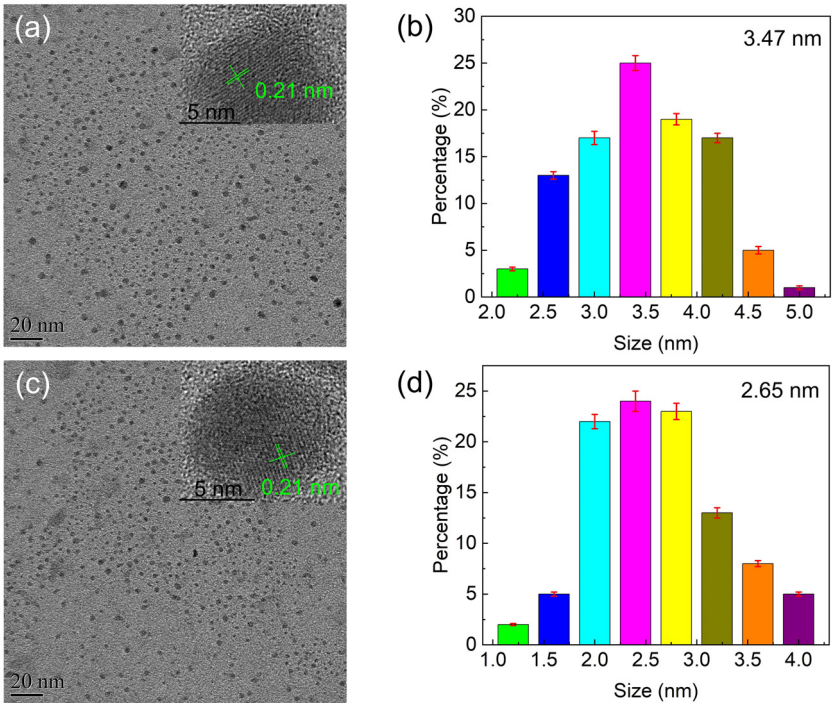

Figure 2: TEM images of (a) RCQDs and (c) SCWE-CQDs, insets are HRTEM images demonstrating the well-dispersive CQDs. The size distribution histograms of (b) RCQDs and (d) SCWE-CQDs show an average diameter of 3.47 and 2.65 nm, respectively.

using TEM and XRD to confirm the chemical structure of CQDs. Figure 2a and c demonstrate the TEM images of RCQDs and SCWE-CQDs, indicating that they are well-dispersive. Additionally, the high-resolution TEM (HR-TEM) image in Figure 2a inset reveals that RCQDs have a conspicuous crystalline characteristic with 0.21 nm lattice distance, corresponding to the (100) lattice planes of graphitic carbon, suggesting the successful synthesis of well-crystallized CQDs. Interestingly, a similar crystal structure was observed in SCWE-CQDs (Figure 2c). Beyond that, the size distribution histograms of RCQDs (Figure 2b) and SCWE-CQDs (Figure 2d) show relatively narrow size distribution, with average diameter of 3.47 and 2.65 nm, respectively. Compared with the SCWE-CQDs, the obtained RCQDs are easy to form "clusters" because of aggregation.

Furthermore, the crystal structures of RCQD and SCWE-CQD were measured by XRD, indicating the typical graphite structure feature of CQDs, with significant diffraction peaks, as shown in Figure 3. The XRD diffraction patterns of RCQDs and SCWE-CQDs show broad diffraction peaks at 21.3° and 21.1°, respectively, indexing as (100) crystal face, which indicated these CQDs are arranged in a disordered order [12]. Additionally, SCWE-CQDs have another sharp diffraction peak at 27.7° due to the stacking of the conjugated aromatic system, corresponding to the (002) crystal face. Based on the above results, it is revealed that the XRD diffraction pattern of SCWE-CQDs is consistent with good crystallization characteristics and the amorphous nature of graphitic carbon [27]. Therefore, these SCWE-CQDs both have crystalline cores and amorphous surfaces simultaneously.

3.2 DMF dilution regulating the optical properties of CQDs

The SCWE-CQDs were prepared by adding a certain amount of DMF into the RCQDs solution, so it is necessary to optimize DMF dilution ratios to obtain SCWE-CQDs with desired

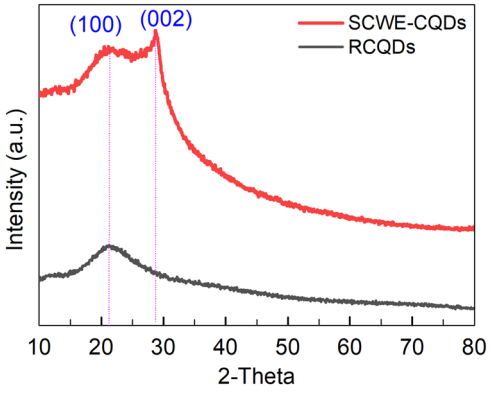

Figure 3: XRD diffraction patterns of RCQDs and SCWE-CQDs.

optical properties. We studied five typical CQDs, which were synthesized by adding different DMF dilution ratios (0, 5, 50, 100, 500 times) to the RCQDs original solution. The optical properties of these products are characterized by UV-visible spectroscopy and photoluminescence spectroscopy. From the result of Figure 4a, these CQDs have different absorption characteristics from UV to visible regions. Without adding DMF, the RCQDs (0 times) have a distinct absorption band at 621 nm. When the dilution ratios are five times, the spectra have two intense absorption bands centered at 536 and 593 nm, respectively. As the dilution ratios increased to 50 and 100 times, the number of absorption peaks changed from two to three, and the first characteristic absorption peak gradually blues shifted. Continuing to increase dilution ratios, four characteristic absorption peaks were observed and the first characteristic absorption peak blue-shifted to the UV region (318 nm). The absorption band less than 350 nm can be attributed to the π–π* interlayer transition of oxygen-functionalized graphitic core or n–π* transitions caused by the CQD "edge band" transition [28]. In addition, the absorption band at 350–800 nm of these products can be assigned to the π–π* aromatic fluorophore structure and the n–π* transitions of the C=O bond [29]. The "edge band" transition refers to a transition between the nonbonding orbital of edge groups to π* orbital of the core in CQDs at the boundary of the sp^2 and sp^3 hybridized carbon, especially in some blue-emitting CQDs, which is similar to many previously reported cases [28,30,31]. The broad absorption band at 486 nm (100 times diluted sample) or longer wavelength can be considered as the "surface band" of CQDs, which probably occur because of the low energy transitions of functional groups attached to the edge of the carbon core [32].

Figure 4b–f show the PL emission spectra of the samples changed under different excitation wavelengths (360–500 nm) excited when the original solution of RCQDs was diluted with DMF by 0, 5, 50, 100, and 500 times, respectively. Figure 4b shows the PL emission spectrum of RCQDs centered at about 675 nm without adding DMF, which appears to be excitation-independent, and the intensity increases with the excitation wavelength range from 360 to 500 nm. When the dilution ratios are five times, the PL emission spectra have two sharp peaks at about 540 and 655 nm, and the peak intensity at 655 nm is significantly higher than that at 540 nm (Figure 4c). Generally, the multi-emissions of CQDs are related to the quantum size effect, surface defect states, and molecular states. In addition, the samples also exhibit excitation-

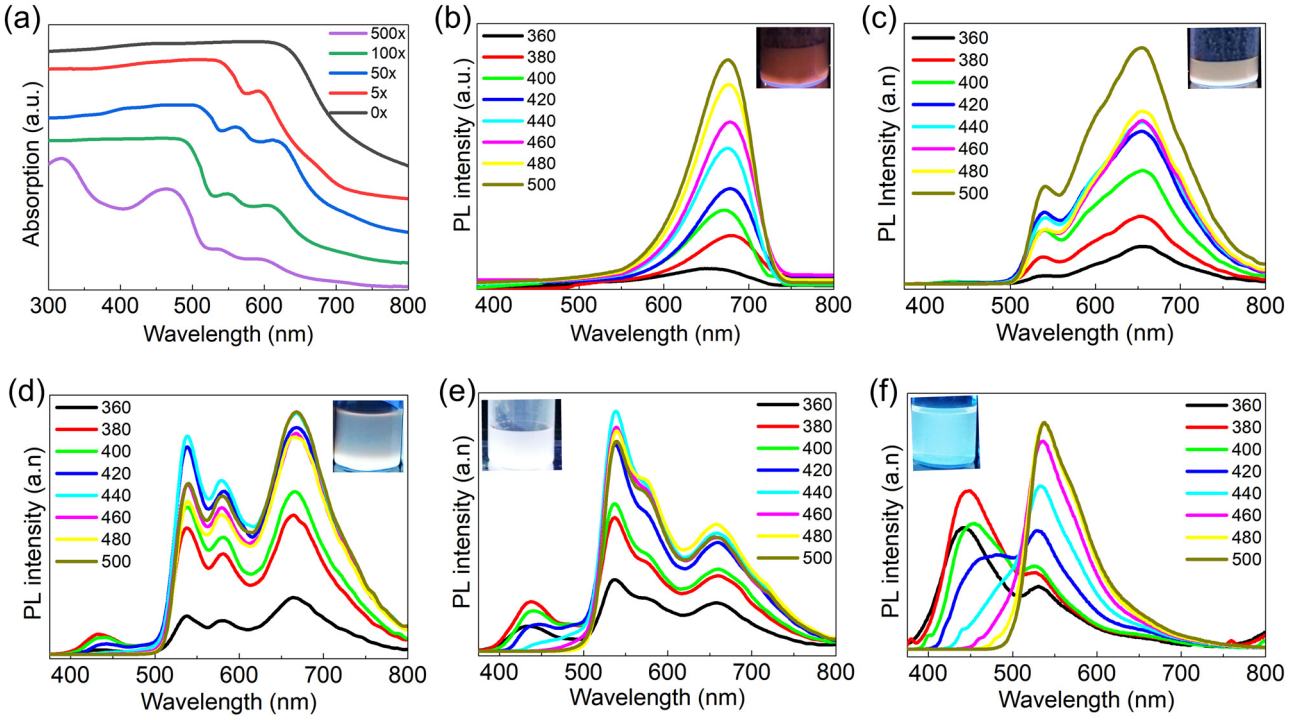

Figure 4: (a) UV-Vis absorption spectra of CQDs synthesized by adding 5 times (red solid line, 5×), 50 time (blue solid line, 50×), 100 times (green solid line, 100×), and 500 times (purple solid line, 500×) DMF dilution ratios into RCQDs solution, and the original RCQDs was denoted as "0" (black solid line), respectively. The PL emission spectra of RCQDs diluted by DMF in (b) 0 times, (c) 5 times, (d) 50 times, (e) 100 times, and (f) 500 times at different excitation wavelengths (360–500 nm), respectively. Insets are photographs of the solutions under 395 nm UV light.

independent behavior. This excitation-independent behavior possibly arises from the different particle sizes and the distribution of molecular states [33,34]. Besides, the TEM images demonstrate that the size distribution of the CQDs ranges from 1.0 to 5.0 nm, which is not very uniform. Therefore, all TEM and FL spectral characteristics indicate that the luminescence of CQDs is related to the particle size, suggesting that there are some particles with different sizes in the solution. As the dilution ratios increase, the PL emission peak position and peak intensity of the sample change obviously. When the dilution ratios are 50 times, the PL emission spectra show three characteristic peaks at 539, 580, and 667 nm, respectively. In addition, the peak intensity of the green region is different from that of the red area, so the color of the solution shows a composite color. When the dilution ratios increase to 100 times, the position of the peaks shifted to 437, 536, and 660 nm, respectively, and the corresponding peak intensities have significant differences. Accordingly, the color of the solution turns to pure white, namely SCWE-CQDs. However, when the dilution ratios further increase, the color of the solution gradually changes to blue, and the PL emission spectrum of CQD shows a double peak and then becomes a single peak as the excitation wavelength is in the range of 360 to 500 nm. These results indicate that the white light of SCWE-CQDs is composed of a mixture of colors. The relative PLQY of the SCWE-CQDs is 53% under 365 nm excitation, demonstrating a higher than most previous reported, as presented in Table 1.

3.3 Determining the relationship between DMF and CQDs

To study the blue shift characteristics caused by DMF induced, FTIR and XPS characterizations were further performed to distinguish the chemical bonding and chemical composition of RCQDs and SCWE-CQDs. As shown in Figure 5a and b, both RCQDs and SCWE-CQDs have a lot of hydrophilic groups such as O–H/N–H (3,450–3,150 cm^{-1}) and C–O (1,260 cm^{-1}) on their surfaces, which make them possess good solubility in water [38]. Furthermore, the stretching vibration band of the C–H (2,935 cm^{-1}), C═N (1,660 cm^{-1}), and C–N (1,398 and 1,460 cm^{-1}) was observed, revealing the formation of polyaromatic structures, which is consistent with absorption and PL emission results [39]. Comparing the FTIR spectra of these samples, we found the enhancement of the typical stretching vibration intensity of O–H/N–H (3,450–3,150 cm^{-1}) and C–H (2,935 cm^{-1}) bonds from the RCQDs to SCWE-CQDs, indicating the SCWE-CQDs with higher hydrophilicity and polarity than RCQDs. Similar characteristics are found in carbon nanotubes [40]. In addition, strong peaks at approximately 1,020–1,085 cm^{-1} and 796 cm^{-1} were observed in SCWE-CQDs, which can be ascribed to Si–CH_2 and Si–O–Si bonds stretching vibrations, respectively [26]. The Si–O–Si bonds can avoid the fluorescence quenching of the CQDs due to their chain network structure, thereby improving the stability of the SCWE-CQDs.

Furthermore, the XPS characterizations were carried out to investigate the chemical composition of CQDs, as demonstrated in Figures 6 and 7. Analogously, five peaks at 100.1, 150.5, 284.8, 399.8, and 531.9 eV in the full spectra of XPS are observed in Figure 6a, corresponding to Si2p, Si2s, C1s, N1s, and O1s of RCQDs and SCWE-CQDs, respectively, which indicate the components of CQDs remain unchanged under DMF diluted. Apart from that, the relative contents of the atoms for these samples were compared as shown in Figure 6b. The XPS intensity at 399.8 eV gradually increases from the RCQDs to SCWE-CQDs, implying a corresponding increase in the number of amide groups in the CQDs, which reconfirms the FTIR analysis results. In addition,

Table 1: Comparison of different methods for synthesizing SCWE-CQDs

Methods	Precursors	Synthesis conditions	PLQY (%)	References
Microwave	l-Aspartic acid, ammonia solution, NaOH	750 W microwave irradiation	6.7	[35]
Solvothermal method	Guanidine carbonate, monopotassium phosphate	170°C for 8 h	10	[36]
Hydrothermal method	Urea	195°C for 10 h	25	[22]
Ultrasonic treatment	Polyamide resin, KH570	Ultrasound for 3 h	28.3	[24]
Hydrothermal method and microwave	Citric acid, urea, sodium silicate	160°C for 4 h, 550 W microwave irradiation for 2 min	30	[2]
Solvothermal method	Ammonium citrate, EDTA, DMF	160°C for 6 h	35.9	[37]
Solvothermal method	Citric acid, urea, CTAB	180°C for 8 h	38.7	[25]
Solvothermal method	O-phenylenediamine, tartaric acid	180°C for 12 h	39	[3]
Solvothermal method	Ammonium citrate, DMF	180°C for 3 h	57.1	[26]
Solvent engineering method	AEAPMS, DMF	Room temperture	53	This work

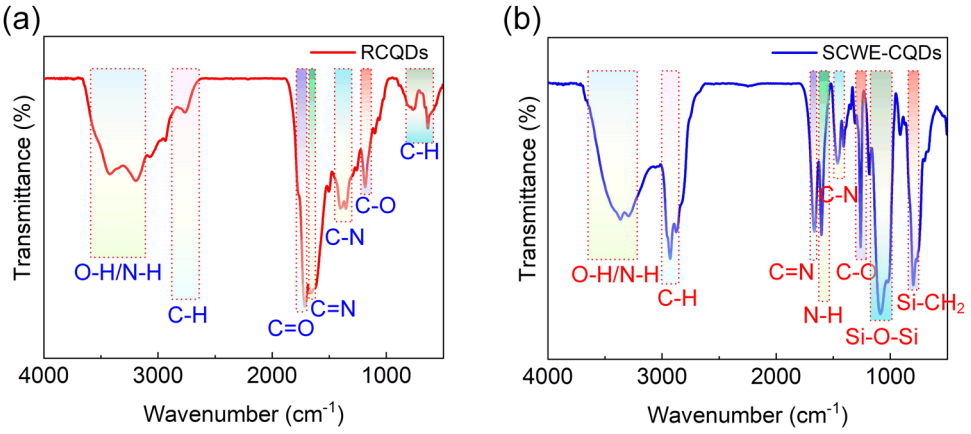

Figure 5: FTIR spectra of (a) RCQDs and (b) SCWE-CQDs.

the high-resolution narrow scan spectra of atoms were recorded, as shown in Figure 7. The C1s band of two typical CQDs can be divided into three peaks, relevant to C–C/C═C (284.7 eV), C–O/C–N (285.7 eV), and C═O (288.2 eV), evidencing that there are sp^2 and sp^3 carbons in these CQDs [41,42]. Accordingly, the N1s band of CQDs can be divided into three peaks, corresponding to C═N (398.9 eV), N–H (399.9 eV), and C–N (401.0 eV). Additionally, the O1s band of CQDs can be decomposed to two peaks of C–O (530.7 eV) and C═O (532.1 eV). All the above results indicate that these CQDs possess abundant functional groups, allowing them highly dissolvable in water and organic solvents, which is meaningful for further applications.

3.4 DMF solvation effect on the fluorescent mechanism

Until now, the mechanism for the PL emission of CQDs can be concluded as follows: (i) the quantum confinement effect or the conjugated π-domains of carbon core, namely intrinsic states; (ii) the surface functional groups concatenated with the carbon skeleton, known as surface states; (iii) the fluorescent molecular group connected on the surface or interior of CQDs, called molecular state [43–45]. Usually, the PL emission of CQDs deriving from intrinsic states or surface states is insensitive to most solvents (*e.g.*, DMF, water). On the contrary, the PL emission originating from molecular states is very sensitive to the solvent environment [46]. According to the characterization of absorption, PL emission, and PLQY of RCQDs and SCWE-CQDs (Figure 4), the optical properties of CQDs depend strongly on the DMF amount, suggesting that the emission of CQDs possibly originates from the molecular states. Based on molecule fluorescence principles, the spectrum shift induced by the solvation effect can be further divided into two classes: general solvation effect and specific solvation effect [46]. The general solvation effect is caused by solvent polarity, while the specific solvation effect is influenced by a combination of many complicated factors, such as hydrogen bonds (HBs), internal charge transfer, and conformational changes [29]. In this article, the spectrum shift is regulated by DMF dilution ratios, thus the specific solvation effect is responsible for the PL spectrum shift. In addition, both the

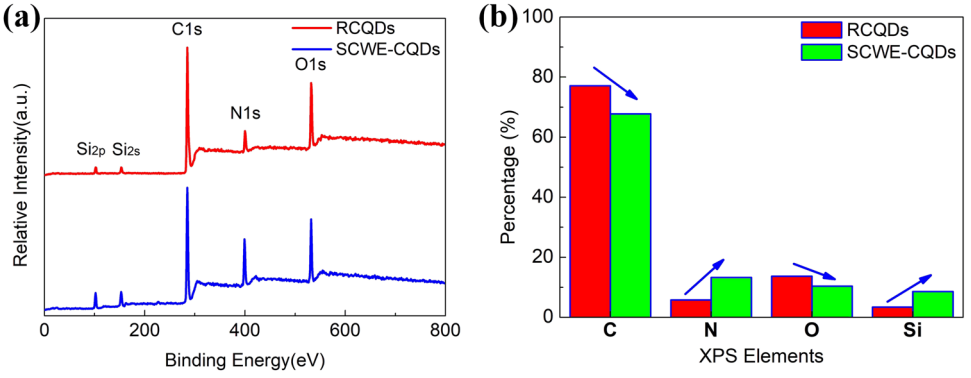

Figure 6: (a) XPS full survey of RCQDs and SCWE-CQDs, (b) XPS elemental analysis results of the RCQDs and SCWE-CQDs.

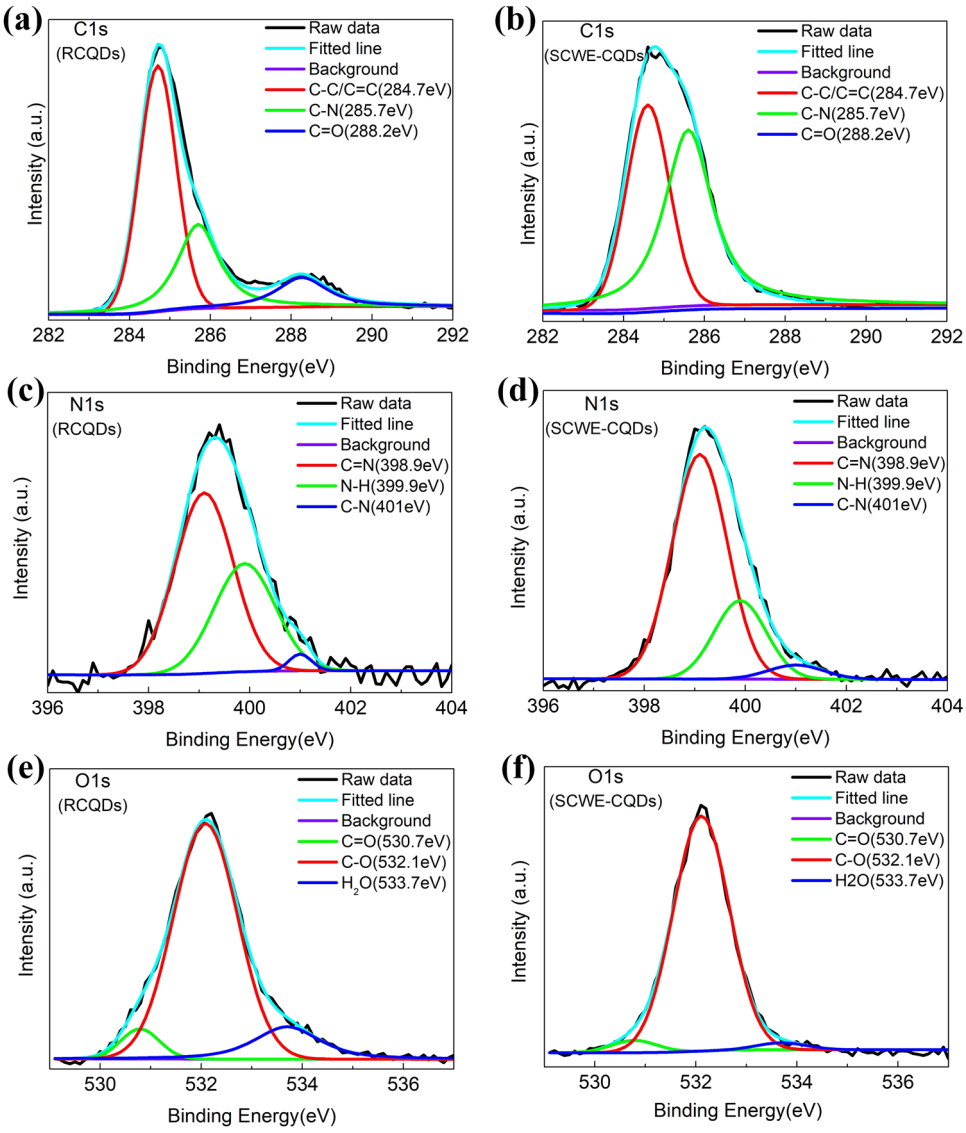

Figure 7: High-resolution narrow scan spectra of (a) C1s, (b) N1s, and (c) O1s for the RCQDs, and (d) C1s, (e) N1s, and (f) O1s for the SCWE-CQDs.

adsorption and PL spectra changes demonstrate that the HB is formed between CQDs and DMF *via* amino or imino groups donating or accepting protons [46]. Lin's group and Song's group confirmed that the specific PL properties of CQDs are caused by the strong HB effect formed in polar aprotic solvents [28,46]. Moreover, the FTIR and XPS results (Figures 5–7) confirmed that the nitrogen atoms were attached to the surface of CQDs in the form of graphitic nitrogen and pyrrolic nitrogen. Therefore, with more DMF added, the exposed nitrogen atoms attached to CQDs surface build a powerful HB with DMF *via* nitrogen protonation. Meanwhile, the electron transmissions can be realized between the hydrogen atom and nitrogen atom by HB donor-to-acceptor bridges. With the HB effect reinforced, the bandgap between the lowest excited singlet state and the ground state increases, resulting in RCQDs blue-shifted and thereby

Table 2: Performance of WLEDs fabricated with different contents of cellulose

Contents of cellulose (g)	CIE coordinates		Luminous efficiency (lm/W)	CCT (K)	CRI
	X	*Y*			
0.05	0.363	0.369	1.55	4,113	87
0.1	0.357	0.359	1.30	4,271	89
0.2	0.339	0.348	1.22	4,811	87
0.3	0.330	0.326	1.14	5,628	82

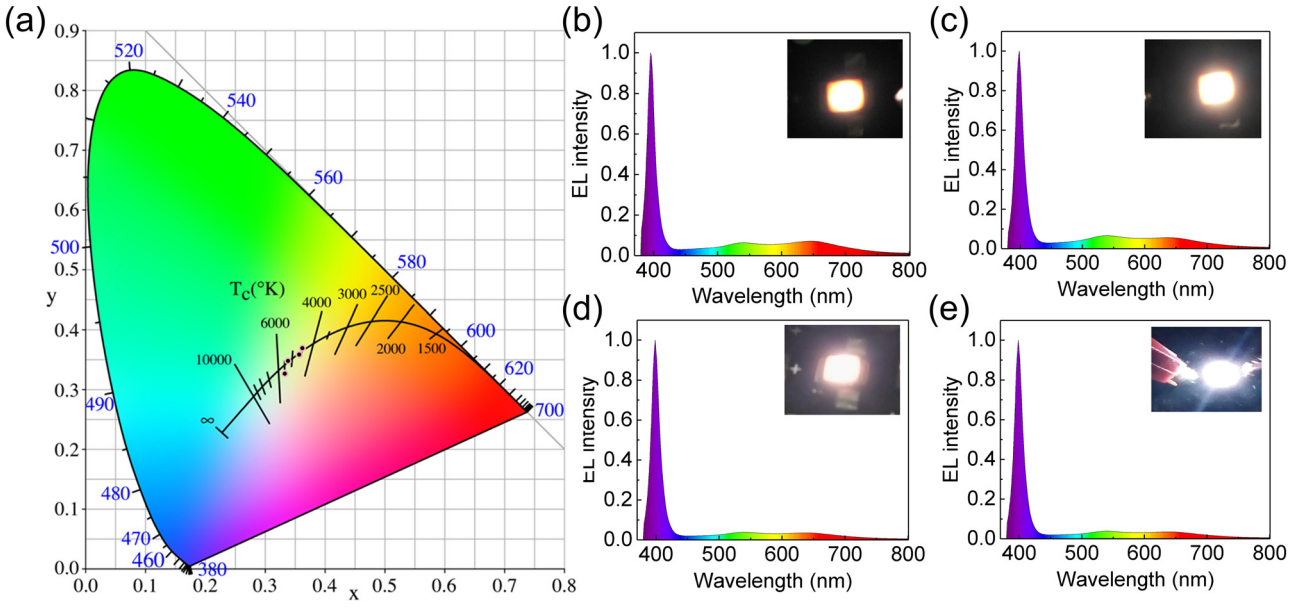

Figure 8: (a) The CIE coordinates of WLEDs, whose structure is composed of 0.05, 0.1, 0.2, and 0.3 g cellulose and UV LED (395 nm) chip. The electroluminescence (EL) patterns of the WLEDs prepared with (b) 0.05 g, (c) 0.1 g, (d) 0.2 g, and (e) 0.3 g of the cellulose, respectively, insets are the working images of devices.

SCWE-CQDs obtained. Additionally, from the results of Figures 2–4, the excitation-independent behavior and the multi-peak characteristics of PL emission of CQDs suggest that the particle sizes affect spectrum shift. However, unlike traditional semiconductor quantum dots, a large CQDs spectral shift (>100 nm) cannot be obtained by simply varying the particle size [47]; in most cases, the large spectral shift is related to the surface electron transmissions rather than the size [48]. In general, the combined action of the HB effect and the size effect leads to the blue shift of RCQDs, but the HB effect is more dominant than the particle size in causing large spectral shifts.

3.5 Performance of WLEDs based on SCWE-CQDs

Regarding high-quality WLEDs' application in displays, optimizing relevant parameters is of great significance for obtaining high CRI and pure white light. During the fabrication of WLEDs devices, we found that the contents of cellulose and SCWE-CQDs have a significant effect on WLEDs' performance. Therefore, we then focused on these two parameters. Initially, the contents of cellulose ranging from 0.05 to 0.3 g are investigated, keeping the content of SCWE-CQDs solution (1.0 mL) unchanged. Table 2 exhibits the performance of the obtained WLEDs, mainly containing the CIE chromaticity coordinates, luminous efficiency, CCT, and CRI. As shown in Table 2, by changing cellulose contents, the CIE color coordinates (0.330–0.363, 0.326–0.369) and CRI of 82–89 acquired in the white light region. In addition, with the increase of cellulose contents, the CIE coordinates are gradually approached pure white light (0.33, 0.33), and CCT also gradually changes from warm light color to cold light color and maintains a high CRI. Furthermore, the relevant electroluminescence (EL) spectra of the as-fabricated WLEDs with different CCTs are demonstrated in Figure 8a–e. With the increase of cellulose contents, the CCT of the WLEDs changes from 4,113 to 5,628 K (Figure 8a). At the same time, the corresponding CRI value at different CCTs did not drop significantly, and the maximum value reached 89, which is potential for micro-display or indicator applications. Besides, it is

Table 3: Performance of WLEDs fabricated by adding different contents of SCWE-CQDs

SCWE-CQDs contents (mL)	CIE coordinates		Luminous efficiency (lm/W)	CCT (K)	CRI
	X	*Y*			
0.2	0.295	0.291	0.85	8,478	81
0.5	0.312	0.319	1.0	6,622	82
0.8	0.328	0.336	1.1	5,710	84
1.1	0.356	0.366	1.3	4,662	85

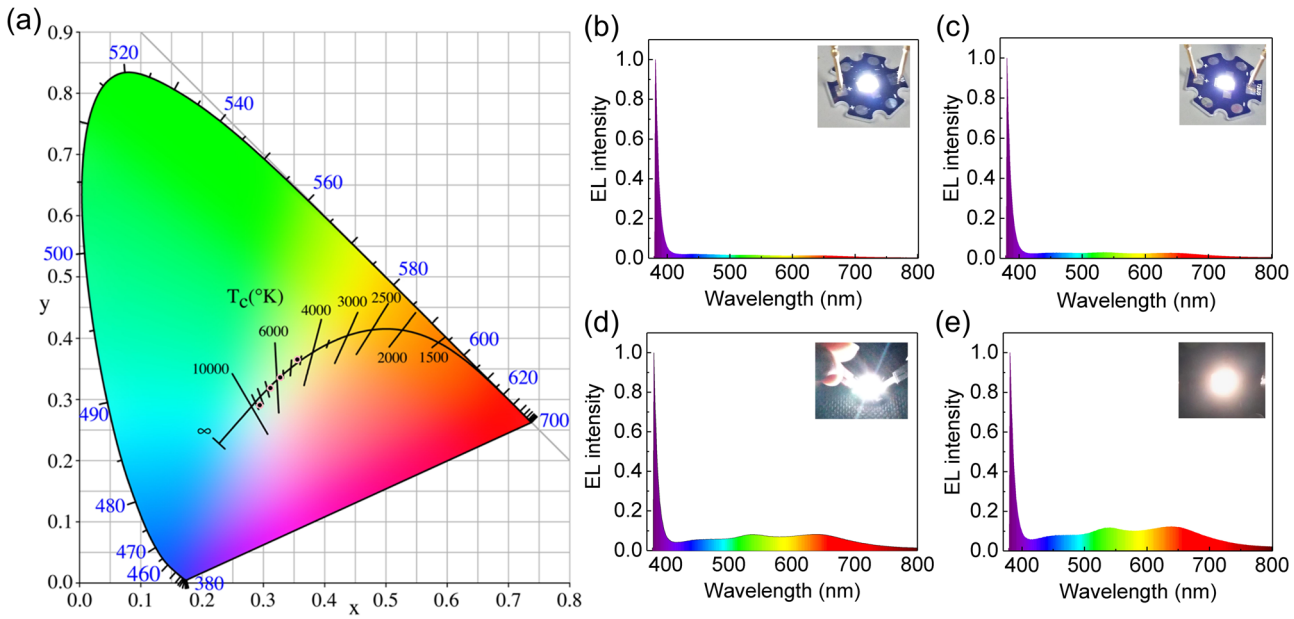

Figure 9: (a) The CIE coordinates of WLEDs, whose structure is composed of 0.2, 0.5, 0.8, and 1.1 mL SCWE-CQDs and UV-LED (395 nm) chip. The electroluminescence (EL) pattern of the WLEDs device prepared by diluting (b) 0.2 mL, (c) 0.5 mL, (d) 0.8 mL, and (e) 1.1 mL of the SCWE-CQDs, insets are the working images of devices.

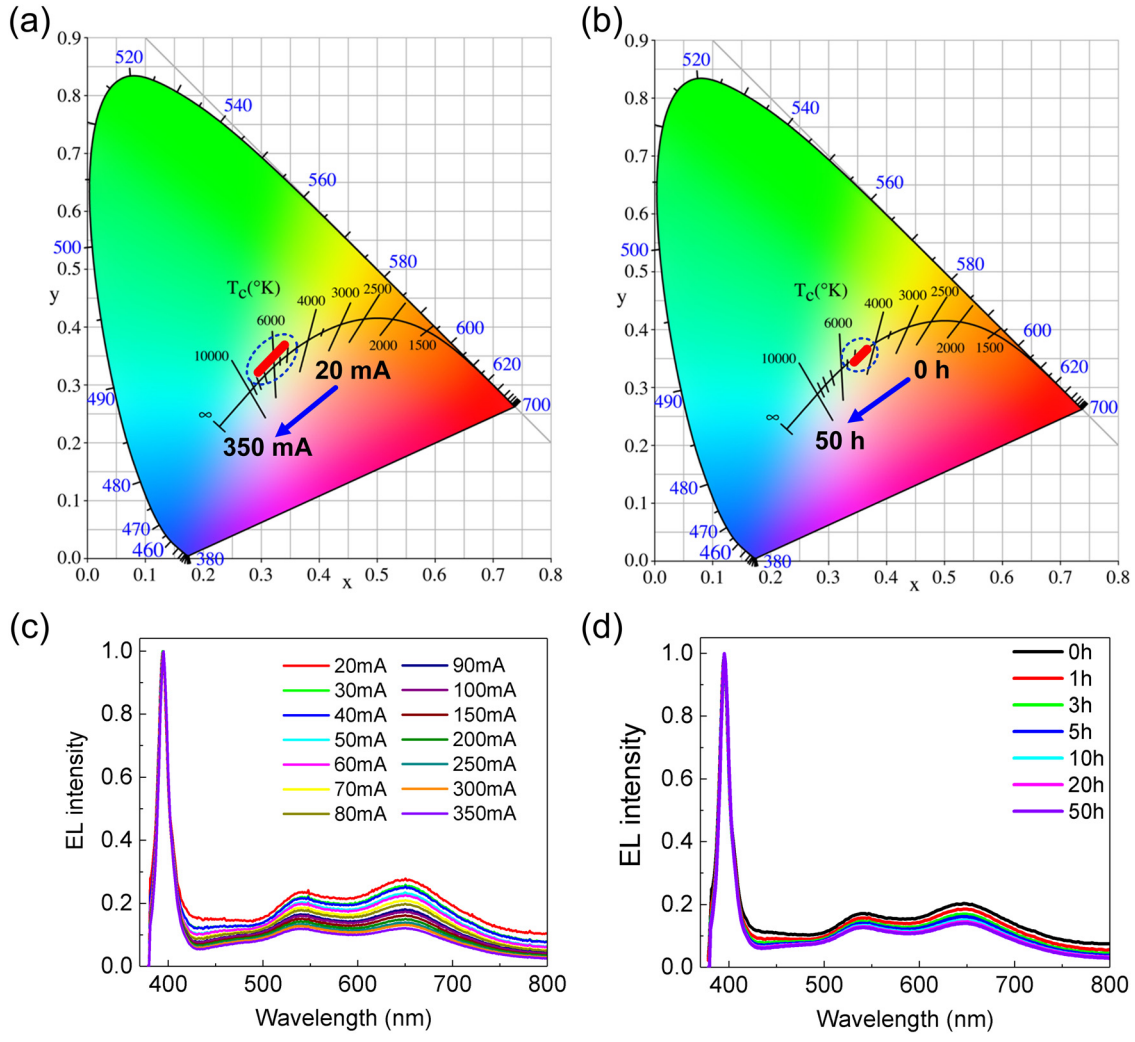

Figure 10: (a) and (c) Variation of color coordinates and EL normalized intensity of WLEDs devices driven by different currents (20–350 mA), (b) and (d) Variation of color coordinates and EL normalized intensity of WLEDs devices under different working times (0–50 h).

worth noting that during the transition from liquid to the solid phase, the PLQY of SCWE-CQDs is significantly reduced due to the aggregation, leading to a decrease in the luminous efficiency of WLEDs. These push us to explore new strategies to alleviate the degradation of fluorescence efficiencies in the liquid-solid phase transition process, such as finite-difference time-domain method and molecular dynamics simulation [49].

Moreover, the effect of the SCWE-CQDs contents on the performance of WLEDs was studied, keeping other conditions the same, as presented in Table 3 and Figure 9. With the SCWE-CQDs contents increased, CIE chromaticity coordinates values, luminous efficiency, and CRI increased, while the CCT values decreased. Importantly, we obtained a white light emission with the CIE coordinates of (0.328, 0.336) approaching pure white light (0.33, 0.33), and corresponding CRI and CCT are 84 and 5,710 K, respectively. Figure 9a shows the CIE coordinates and CCT of WLEDs devices; the CIE coordinates of all devices are near the Planck Black Body radiation curve, which indicates that the WLEDs have a high CRI value, corresponding to Table 3. In addition, Figure 9b–e demonstrate the EL diagram of the normalized drive current of various devices at 20 mA, where the insets are the working images of WELDs devices. Similarly, with the increase of SCWE-CQDs contents, the ratio of long-wavelength in EL spectrum increased, and thereby the CRI increased. These results demonstrate that the SCWE-CQDs are promising to improve the color design of WLEDs for the green light source.

Stability is an important index to value the reliability of WLEDs devices [50]. We use the CIE coordinates pattern and EL spectrum to evaluate the stability of SCWE-CQDs-based WLEDs devices under different working current drives and working time intervals. As shown in Figure 10a and c, although the CIE coordinates of WLEDs devices change greatly within the working current of 20–350 mA, the spectral shape of EL remains unchanged, indicating that WLEDs have excellent current stability. In addition, the time stability of the device within 0–50 h was investigated (Figure 10b and d), and it was found that the CIE coordinates and EL spectrum of these devices did not fluctuate much, indicating that the whole WLEDs device presented good time stability. At the same time, with the increase of working current or the extension of working time, the intensity of the two peaks of the EL spectrum in the green and red regions decreases slightly as SCWE-CQDs are easily affected by the temperature, which leads to the decrease of fluorescence efficiency.

4 Conclusion

To sum up, we get rapid and facile synthesis of highly photoluminescent SCWE-CQDs by controlling the dilution ratios between DMF and the original RCQDs solution. The PLQY of as-prepared SCWE-CQDs reached 53%. Detailed characterization of TEM, XRD, UV-Vis, PL, FTIR, and XPS confirmed that the combined action of the HB effect and the size effect leads to the blue shift of RCQDs, but the HB effect is more dominant than the particle size in causing large spectral shifts. Meanwhile, the electron transport can be realized between the hydrogen atoms and nitrogen atoms by HB donor-to-acceptor bridges. With the enhancement of the HB effect, the bandgap between the lowest excited singlet state and the ground state increases, resulting in a blue shift of the RCQD, thereby obtaining SCWE-CQD. In addition, AEAPMS was chosen as the dispersing medium and protective material to avoid fluorescence self-quenching of the SCWE-CQDs. By optimizing the content of cellulose and SCWE-CQDs, the WLEDs with high CRI (up to 89) and reliability were obtained. Our finding establishes a versatile technique for desirable optical properties of carbon and related nanomaterials by solvent engineering.

Funding information: This project was supported by STU Scientific Research Foundation for Talents (NTF19045, NTF20010), National Natural Science Foundation of China (NSFC, 52005314), General Program of Natural Science Foundation of Guangdong Province (2021A1515010662), and Characteristic Innovation Projects of Ordinary Colleges and Universities in Guangdong Province (2020KTSCX038).

Author contributions: All authors have accepted responsibility for the entire content of this manuscript and approved its submission.

Conflict of interest: The authors declare no conflict of interest.

References

[1] Rao L, Tang Y, Li Z, Ding X, Li J, Yu S, et al. Effect of ZnO nanostructures on the optical properties of white light-emitting diodes. Opt Express. 2017;25(8):A432–43.
[2] Tian Z, Tian P, Zhou X, Zhou G, Mei S, Zhang W, et al. Ultraviolet-pumped white light emissive carbon dot based phosphors for light-emitting devices and visible light communication. Nanoscale. 2019;11(8):3489–94.

[3] Wang L, Li W, Yin L, Liu Y, Guo H, Lai J, et al. Full-color fluorescent carbon quantum dots. Sci Adv. 2020;6(40):eabb6772.
[4] Li J, Tang Y, Li Z, Li J, Ding X, Yu B, et al. Toward 200 lumens per watt of quantum-dot white-light-emitting diodes by reducing reabsorption loss. ACS Nano. 2020;15(1):550–62.
[5] Li Z, Chen Y, Li J, Liang S, Tang Y. Toward one-hundred-watt-level applications of quantum dot converters in high-power light-emitting diode system using water-cooling remote structure. Appl Therm Eng. 2020;179:115666.
[6] Li Z, Zheng J, Li J, Zhan W, Tang Y. Efficiency enhancement of quantum dot-phosphor hybrid white-light-emitting diodes using a centrifugation-based quasi-horizontal separation structure. Opt Express. 2020;28(9):13279–89.
[7] Wang Z, Liu Y, Zhen S, Li X, Zhang W, Sun X, et al. Gram-scale synthesis of 41% efficient single-component white-light-emissive carbonized polymer dots with hybrid fluorescence/phosphorescence for white light-emitting diodes. Adv Sci. 2020;7(4):1902688.
[8] Zhuang Z, Guo X, Liu B, Hu F, Li Y, Tao T, et al. High color rendering index hybrid III-nitride/nanocrystals white light-emitting diodes. Adv Funct Mater. 2016;26(1):36–43.
[9] Jia F, Li G, Yang B, Yu B, Shen Y, Cong H. Investigation of rare earth upconversion fluorescent nanoparticles in biomedical field. Nanotechnol Rev. 2019;8(1):1–17.
[10] Xie Z, Chen C, Xu S, Li J, Zhang Y, Liu S, et al. White-light emission strategy of a single organic compound with aggregation-induced emission and delayed fluorescence properties. Angew Chem Int Edit. 2015;54(24):7181–4.
[11] Mao Z, Yang Z, Mu Y, Zhang Y, Wang Y, Chi Z, et al. Linearly tunable emission colors obtained from a fluorescent-phosphorescent dual-emission compound by mechanical stimuli. Angew Chem. 2015;127(21):6368–71.
[12] Huang Y, Lin H, Qiu J, Luo Z, Yao Z, Liu L, et al. High color rendering indices of white light-emitting diodes based on environmentally friendly carbon and AIZS nanoparticles. J Mater Chem C. 2020;8(23):7734–40.
[13] Kim TH, White AR, Sirdaarta JP, Ji W, Cock IE, St John J, et al. Yellow-emitting carbon nanodots and their flexible and transparent films for white LEDs. ACS Appl Mater Inter. 2016;8(48):33102–11.
[14] Liang T, Liu E, Li M, Ushakova EV, Kershaw SV, Rogach AL, et al. Morphology control of luminescent carbon nanomaterials: from dots to rolls and belts. ACS Nano. 2020;15:1579–89.
[15] Wojtera K, Walczak M, Pietrzak L, Fraczyk J, Szymanski L, Sobczyk-Guzenda A. Synthesis of functionalized carbon nanotubes for fluorescent biosensors. Nanotechnol Rev. 2020;9(1):1237–44.
[16] Pachfule P, Shinde D, Majumder M, Xu Q. Fabrication of carbon nanorods and graphene nanoribbons from a metal-organic framework. Nat Chem. 2016;8(7):718–24.
[17] Visconti P, Primiceri P, de Fazio R, Strafella L, Ficarella A, Carlucci AP. Light-induced ignition of carbon nanotubes and energetic nano-materials: a review on methods and advanced technical solutions for nanoparticles-enriched fuels combustion. Rev Adv Mater Sci. 2020;59(1):26–46.
[18] Tang Y, Rao L, Li Z, Lu H, Yan C, Yu S, et al. Rapid synthesis of highly photoluminescent nitrogen-doped carbon quantum dots via a microreactor with foamy copper for the detection of Hg^{2+} ions. Sensor Actuat B Chem. 2018;258:637–47.
[19] Rao L, Tang Y, Li Z, Ding X, Liang G, Lu H, et al. Efficient synthesis of highly fluorescent carbon dots by microreactor method and their application in Fe^{3+} ion detection. Mat Sci Eng C Mater. 2017;81:213–23.
[20] Rao L, Tang Y, Lu H, Yu S, Ding X, Xu K, et al. Highly photoluminescent and stable N-doped carbon dots as nanoprobes for Hg^{2+} detection. Nanomaterials (Basel). 2018;8(11):900.
[21] He P, Shi Y, Meng T, Yuan T, Li Y, Li X, et al. Recent advances in white light-emitting diodes of carbon quantum dots. Nanoscale. 2020;12(8):4826–32.
[22] Yuan T, Yuan F, Li X, Li Y, Fan L, Yang S. Fluorescence-phosphorescence dual emissive carbon nitride quantum dots show 25% white emission efficiency enabling single-component WLEDs. Chem Sci. 2019;10(42):9801–6.
[23] He J, He Y, Chen Y, Lei B, Zhuang J, Xiao Y, et al. Solid-state carbon dots with red fluorescence and efficient construction of dual-fluorescence morphologies. Small. 2017;13(26):1700075.
[24] Dang H, Huang L-K, Zhang Y, Wang C-F, Chen S. Large-scale ultrasonic fabrication of white fluorescent carbon dots. Ind Eng Chem Res. 2016;55(18):5335–41.
[25] Zhu J, Bai X, Zhai Y, Chen X, Zhu Y, Pan G, et al. Carbon dots with efficient solid-state photoluminescence towards white light-emitting diodes. J Mater Chem C. 2017;5(44):11416–20.
[26] Zhang Y, Feng J, He M, Jiang J, Xu T, Zhou L, et al. Efficient and stable white fluorescent carbon dots and CD-based glass thin-films via screen-printing technology for use in W-LEDs. RSC Adv. 2017;7(78):49542–7.
[27] Dassan EGB, Ab Rahman AA, Abidin MSZ, Akil HM. Carbon nanotube-reinforced polymer composite for electromagnetic interference application: a review. Nanotechnol Rev. 2020;9(1):768–88.
[28] Chen Y, Lian H, Wei Y, He X, Chen Y, Wang B, et al. Concentration-induced multi-colored emissions in carbon dots: origination from triple fluorescent centers. Nanoscale. 2018;10(14):6734–43.
[29] Zhu P, Tan K, Chen Q, Xiong J, Gao L. Origins of efficient multi-emission luminescence in carbon dots. Chem Mater. 2019;31(13):4732–42.
[30] Sharma A, Gadly T, Gupta A, Ballal A, Ghosh SK, Kumbhakar M. Origin of excitation dependent fluorescence in carbon nanodots. J Phys Chem Lett. 2016;7(18):3695–702.
[31] Wibrianto A, Khairunisa SQ, Sakti SC, Ni'mah YL, Purwanto B, Fahmi MZ. Comparison of the effects of synthesis methods of B, N, S, and P-doped carbon dots with high photoluminescence properties on HeLa tumor cells. RSC Adv. 2021;11(2):1098–108.
[32] Arshad F, Pal A, Rahman MA, Ali M, Khan JA, Sk MP. Insights on the solvatochromic effects in N-doped yellow-orange emissive carbon dots. New J Chem. 2018;42(24):19837–43.
[33] Baragau I-A, Power NP, Morgan DJ, Heil T, Lobo RA, Roberts CS, et al. Continuous hydrothermal flow synthesis of blue-luminescent, excitation-independent nitrogen-doped carbon quantum dots as nanosensors. J Mater Chem A. 2020;8(6):3270–9.
[34] Jiao Y, Gong X, Han H, Gao Y, Lu W, Liu Y, et al. Facile synthesis of orange fluorescence carbon dots with excitation independent emission for pH sensing and cellular imaging. Anal Chim Acta. 2018;1042:125–32.
[35] Feng X, Jiang K, Zeng H, Lin H. A facile approach to solid-state white emissive carbon dots and their application in

UV-excitable and single-component-based white LEDs. Nanomaterials (Basel). 2019;9(5):725.
[36] Meng T, Yuan T, Li X, Li Y, Fan L, Yang S. Ultrabroad-band, red sufficient, solid white emission from carbon quantum dot aggregation for single component warm white light emitting diodes with a 91 high color rendering index. Chem Commun. 2019;55(46):6531–4.
[37] Zhang Y, Yuan R, He M, Hu G, Jiang J, Xu T, et al. Multicolour nitrogen-doped carbon dots: tunable photoluminescence and sandwich fluorescent glass-based light-emitting diodes. Nanoscale. 2017;9(45):17849–58.
[38] Guo J, Li H, Ling L, Li G, Cheng R, Lu X, et al. Green synthesis of carbon dots toward anti-counterfeiting. ACS Sustain Chem Eng. 2019;8(3):1566–72.
[39] Wang H, Sun C, Chen X, Zhang Y, Colvin VL, Rice Q, et al. Excitation wavelength independent visible color emission of carbon dots. Nanoscale. 2017;9(5):1909–15.
[40] Zhang Y-F, Du F-P, Chen L, Yeung K-W, Dong Y, Law W-C, et al. Supramolecular ionic polymer/carbon nanotube composite hydrogels with enhanced electromechanical performance. Nanotechnol Rev. 2020;9(1):478–88.
[41] Wang CF, Cheng R, Ji WQ, Ma K, Ling L, Chen S. Recognition of latent fingerprints and ink-free printing derived from interfacial segregation of carbon dots. ACS Appl Mater Inter. 2018;10(45):39205–13.
[42] Chen D, Gao H, Chen X, Fang G, Yuan S, Yuan Y. Excitation-independent dual-color carbon dots: surface-state controlling and solid-state lighting. ACS Photonics. 2017;4(9):2352–8.
[43] Sharma A, Gadly T, Neogy S, Ghosh SK, Kumbhakar M. Molecular origin and self-assembly of fluorescent carbon nanodots in polar solvents. J Phys Chem Lett. 2017;8(5):1044–52.
[44] Zhu S, Song Y, Zhao X, Shao J, Zhang J, Yang B. The photoluminescence mechanism in carbon dots (graphene quantum dots, carbon nanodots, and polymer dots): current state and future perspective. Nano Res. 2015;8(2):355–81.
[45] Madhu M, Chen TH, Tseng WL. White-light emission of single carbon dots prepared by hydrothermal carbonization of poly (diallyldimethylammonium chloride): Applications to fabrication of white-light-emitting films. J Colloid Interf Sci. 2019;556:120–7.
[46] Zhang T, Zhu J, Zhai Y, Wang H, Bai X, Dong B, et al. A novel mechanism for red emission carbon dots: hydrogen bond dominated molecular states emission. Nanoscale. 2017;9(35):13042–51.
[47] Eda G, Lin YY, Mattevi C, Yamaguchi H, Chen HA, Chen IS, et al. Blue photoluminescence from chemically derived graphene oxide. Adv Mater. 2010;22(4):505–9.
[48] Shamsipur M, Barati A, Karami S. Long-wavelength, multicolor, and white-light emitting carbon-based dots: achievements made, challenges remaining, and applications. Carbon. 2017;124:429–72.
[49] Yin J, Han J, Qi C, Wang Y. Arrangement structure of carbon nanofiber with excellent spectral radiation characteristics. Nanotechnol Rev. 2020;9(1):789–99.
[50] Rao L, Tang Y, Yan C, Li J, Zhong G, Tang K, et al. Tuning the emission spectrum of highly stable cesium lead halide perovskite nanocrystals through poly (lactic acid)-assisted anion-exchange reactions. J Mater Chem C. 2018;6(20):5375–83.